




Large Eddy Simulation-Based Turbulent Combustion Models for Reactive Sprays: Recent Advances and Future Challenges

Eshan Sharma and Santanu De^{*} 

Abstract | Numerical simulations of turbulent reactive sprays are challenging owing to the presence of multiple timescales and multiphysics phenomena involving complex turbulence spray and turbulence-chemistry interactions. In turbulent spray flames, several physical phenomena such as primary and secondary atomization, droplet dispersion, interparticle collisions, evaporation, mixing, and combustion occur simultaneously, and hence it becomes a formidable task to model these complex interactions. To gain fundamental knowledge and advance current modeling capabilities, it may be appropriate to aim for progress in individual modeling of breakup, dispersion, mixing and combustion, which however cannot be viewed in complete isolation. A brief review of the development of state-of-the-art turbulent combustion models applicable to the dilute spray regime is presented. Therefore, complexities associated with the dense regime, including interparticle collisions as well as primary and secondary atomization, are not covered. Further, we restrict ourselves to a brief discussion on large eddy simulation, which has found applications in both laboratory and industrial applications of turbulent combustion without a change in phase. The gas phase-based turbulent combustion models such as flamelet, conditional moment closure and transported filtered density function methods have been developed and extensively used for combustion without a phase change. However, careful adaptation and extension of these models are necessary toward modeling of turbulent combustion with phase change. This article presents a review of recent advances and directions of future research on modeling of turbulent combustion for dilute sprays.

Keywords: *Spray combustion, Turbulent combustion, Large eddy simulation, Filtered density function, Mixture fraction, Evaporation*

1 Introduction

Intense turbulence-chemistry interactions with a change in phase are predominant in many engineering devices, such as liquid-fueled furnaces, gas turbines, direct injection, and rocket injection engines. Due to the high energy density, combustion of liquid hydrocarbons is expected to continue for both land- and air-based transportation

systems in the foreseeable future. Liquid fuel often injected as a thin column or sheet eventually disintegrates to produce a large number of fine, dispersed liquid droplets. These droplets undergo dispersion and evaporation as they move under the influence of the gas phase and subsequently evaporated fuel mixes with the surrounding oxidizer leading to combustion.

¹ Department of Mechanical Engineering, Indian Institute of Technology, Kanpur 208016, India.
^{*}sde@iitk.ac.in

While turbulence remains as one of the unresolved problems in classical physics, conversion of chemical to thermal energy through a myriad of chemical reactions in a turbulent flow field poses unparalleled complexities associated with fundamental understanding and predictive modeling of highly nonlinear turbulence chemistry and turbulence spray interactions. Therefore, numerical simulations of turbulent reacting sprays rely heavily on the accurate description of primary and secondary atomization, droplet dispersion and evaporation under the influence of underlying turbulent flows, as they are considered to be the rate-limiting process¹.

Turbulence modeling approaches, such as direct numerical simulations (DNS), large eddy simulations (LES) and Reynolds-averaged Navier–Stokes (RANS) have been used to model spray combustion. A Eulerian-Lagrangian approach², where the droplets are tracked in the Lagrangian frame using Newton's equation of motion and the gas phase in the Eulerian frame, is mostly used to model dilute sprays. In this approach, a 'point-particle' assumption is made, where the dispersed, particle phase is assumed to be of the order of the subgrid size. In the context of LES, these subgrid size droplets interact with underlying subgrid turbulence, and hence the droplet modeling should reflect the effects of these unresolved subgrid-scale fluctuations of flow variables on droplet dispersion and inter-phase transfer rates. LES is a three-dimensional, unsteady computational technique where the unsteady Navier–Stokes equations are spatially filtered, the large scales of the flow are directly computed after removing the instantaneous small-scale fluctuations by the filter and the influence of the unresolved, subgrid scales on the resolved scales is accounted using subgrid-scale stresses/fluxes. LES of turbulent combustion has only emerged as a science in the 1990s, and over the last two decades, it has been applied to a wide variety of combustion problems of both practical and research interests³. However, in the literature, there are only very limited instances of LES applied to turbulent reacting and nonreacting sprays compared to LES of gas-phase combustion. In this review article, we briefly present the state-of-the-art modeling approaches of spray combustion based on LES.

Models for turbulent combustion may be classified into two broad categories: mixture fraction-based presumed filtered density function (FDF) approach, and the transported FDF approach. The mixture fraction concept has been routinely used for advancing our understanding on mixing

and combustion processes for non-premixed turbulent flows without a phase change and led to the development of several advanced modeling approaches for turbulent reactive flows. In mixture fraction-based presumed FDF approaches, the instantaneous state relationship of reactive scalars with mixture fraction may be specified at different levels of difficulties: a burning profile based on infinite fast chemistry or Burke–Schumann limit⁴, flamelet model⁵ and the conditional moment closure (CMC) model^{6,7}, while the FDF of mixture fraction may be conveniently assumed by β function. For reactive flows with phase change, the mixture fraction no longer remains a conserved scalar and the choice of the often used presumed β -pdf may be a questionable assumption for spray combustion due to evaporation of droplets^{1,8,9}. On the other hand, in the transported FDF method, the turbulent flow field is described by the transport equation of composition FDF or joint FDF of the velocity and scalars (species mass fractions, enthalpy/temperature). In the transported FDF formulation, the nonlinear chemical source term does not require any closure, although the terms describing molecular mixing or micro-mixing term in the reactive scalar space, fluctuating pressure term and transport of FDF in the velocity space by viscous stresses require closure models^{10–12}.

Numerical simulations of dilute spray combustion have been successfully performed in the past^{1,13–17}. However, an improper choice of inlet boundary condition could lead to inaccurate predictions. To develop and validate numerical models for turbulent combustion, well-defined inlet boundary conditions should be supplied. In this review article, we present results from recent simulations of spray jet flames investigated at the University of Sydney^{18–20}. These burners operate on the dilute spray regime, and hence complexities associated with atomization, secondary breakup, droplet collisions, and coalescence can be neglected. Due to well-defined inlet conditions, these spray burners are suitable for development and validation of turbulent spray combustion models, where the primary focus lies in modeling turbulence spray and turbulence-chemistry interactions.

Herein, a review of the state-of-the-art turbulent combustion models for dilute reactive sprays is presented. The remainder of this chapter is organized as follows. In Sect. 2, the governing equations of continuous phase are briefly presented for dilute spray flames, followed by the governing equations for dilute sprays in Sect. 3. In Sects. 4 and 5, mixture fraction-based presumed FDF models and the transported FDF methods are described,

respectively. In Sect. 6, results from some of the recent numerical studies on the Sydney spray flames have been presented using various combustion models. Finally, major conclusions and future research directions are summarized in Sect. 7.

2 Governing Equations of the Continuous Phase

In this section, we briefly present the gas phase-governing equations within the LES framework for variable density, low Mach number, dilute reactive sprays by neglecting the acoustic interactions and compressibility effects. To account for the density variation, density-weighted (or Favre) filtering is used for all flow variables except those that depend on the mass of the system, e.g., density and pressure. For any flow field variable ϕ , Favre-averaged quantity is written as:

$$\tilde{\phi} = \frac{\overline{\rho\phi}}{\bar{\rho}}, \tag{1}$$

where the overbar designates ordinary filtering, and the tilde specifies mass-weighted filtering. In LES, the instantaneous field variables are decomposed into resolved and subgrid-scale quantities as $\phi = \tilde{\phi} + \phi'$. The LES equations are obtained by applying this decomposition on the governing equations, and subsequently applying the grid filter to the resulting equations. The large-scale or resolved fields are related to the instantaneous field via a filtering function G :

$$\tilde{\phi}(x, t) = \frac{1}{\bar{\rho}} \int_V \rho(y, t) \phi(y, t) G(x - y) dy, \tag{2}$$

where the integral is over the entire computational domain V and the filter function satisfies $\int_V G(y) dy = 1$ and $G(y) = G(-y)$. The filter function G has a filter width Δ , which may vary with position. It is desirable to have G as a positive definite function, so that a subgrid FDF may be defined. Although the small-scale fluctuations are removed by the filter, the influence of the unresolved subgrid scales on the resolved scales is modeled in terms of the subgrid-scale stresses/fluxes. For dilute reacting sprays, the filtered Navier–Stokes equations can be written as:

$$\frac{\partial \bar{\rho}}{\partial t} + \frac{\partial}{\partial x_j} (\bar{\rho} \tilde{u}_j) = \bar{S}_\rho, \tag{3}$$

$$\begin{aligned} \frac{\partial}{\partial t} (\bar{\rho} \tilde{u}_i) + \frac{\partial}{\partial x_j} (\bar{\rho} \tilde{u}_i \tilde{u}_j) &= -\frac{\partial \bar{p}}{\partial x_i} \\ &+ \frac{\partial}{\partial x_j} (2\bar{\mu} \tilde{S}_{ij}) - \frac{\partial \tau_{ij}^{sgs}}{\partial x_j} + \bar{S}_{u_i}, \end{aligned} \tag{4}$$

where \tilde{u}_i is the density-weighted filtered velocity of the gas phase, and $\bar{\rho}$ and \bar{p} are the filtered density and pressure, respectively.

The subfilter stresses, $\tau_{ij}^{sgs} = \bar{\rho} \tilde{u}_i \tilde{u}_j - \bar{\rho} \tilde{u}_i \tilde{u}_j$, is popularly modeled using eddy viscosity-based models such as the Smagorinsky model²¹, the dynamic Smagorinsky model of Germano-Lilly²²,²³ and the wall-adapting local eddy (WALE) viscosity model²⁴. In the dynamic Smagorinsky model²², the deviatoric part of the subgrid stress is related to the filtered strain tensor tensor via $\tau_{ij}^{sgs} = -2\mu_{sgs} \tilde{S}_{ij}$, where Lagrangian averaging technique²⁵ is often used for averaging along a streamline. The subgrid scale (SGS) viscosity is modeled as $\mu_{sgs} = \bar{\rho} (C_{sgs} \Delta^2) \|\tilde{S}_{ij}\|$. The Smagorinsky constant C_{sgs} is determined by the dynamic procedure²². Here, the filtered strain rate tensor is given as $\tilde{S}_{ij} = \frac{1}{2} \left(\frac{\partial \tilde{u}_i}{\partial x_j} + \frac{\partial \tilde{u}_j}{\partial x_i} \right)$, and the Frobenius norm of the strain rate tensor as $\|\tilde{S}_{ij}\| = \sqrt{2\tilde{S}_{ij}\tilde{S}_{ij}}$. The modeling of the filtered interphase transfer terms, \bar{S}_ρ and \bar{S}_{u_i} , is discussed in the next section. A transport equation of energy is often solved separately to obtain the gas phase temperature field,

$$\begin{aligned} \frac{\partial}{\partial t} (\bar{\rho} \tilde{h}) + \frac{\partial}{\partial x_j} (\bar{\rho} \tilde{u}_j \tilde{h}) &= \frac{\partial}{\partial x_j} \left(\lambda \frac{\partial T}{\partial x_j} \right) \\ &- \frac{\partial q_{j,h}^{sgs}}{\partial x_j} + \bar{\omega}_h + \bar{S}_h, \end{aligned} \tag{5}$$

where λ is the thermal conductivity of the gas, $\bar{\omega}_h$ is the energy source term due to chemical reaction and \bar{S}_h is the filtered source term due to heat exchange between discrete phase and the continuous phase. The subfilter heat flux, $q_{j,h}^{sgs} = \bar{\rho} \tilde{u}_j \tilde{h} - \bar{\rho} \tilde{u}_j \tilde{h}$, may be modeled using the gradient approximation as $q_{j,h}^{sgs} = -\frac{\mu_{sgs}}{Pr_t} \frac{\partial \tilde{h}}{\partial x_j}$, where Pr_t is the turbulent Prandtl number. The viscous dissipation and the pressure contribution terms are neglected in Eq. (5).

3 Modeling of the Dispersed Phase

The dispersed liquid phase is most often modeled based on the stochastic particle method (SPM), in which the liquid phase is represented by a large number of discrete computational parcels. Each computational parcel consists of a finite number of droplets N_d , with identical properties, e.g., the d -th parcel consists of droplets with identical location (x_d), diameter (D_d), velocity (v_d) and temperature (T_d). The uniform temperature or the infinite liquid conductivity thermal model of Abramzon and Sirignano²⁶ is often used in the literature to describe evaporation^{1, 9, 14, 27}. The effect

of radiation on droplet heating and evaporation may be neglected, although the use of a uniform radiation absorption model for spray combustion has been recommended²⁸. In SPM, the liquid droplets are tracked following the Lagrangian framework. For dilute sprays, both droplet-droplet interaction and coalescence may be neglected. The governing equations for the individual droplets are expressed as^{2,29}:

$$\frac{dx_d}{dt} = v_d, \tag{6}$$

$$\frac{dv_d}{dt} = f_1 \frac{u_d^g - v_d}{\tau_d} + \left(1 - \frac{\rho_g}{\rho_l}\right)g, \tag{7}$$

$$\frac{dT_d}{dt} = \frac{NuC_p^g}{3PrC_p^l} \left(\frac{T_d^g - T_d}{\tau_d}\right) \frac{\ln(1 + B_H)}{B_H} + \frac{\dot{m}_d L_v}{m_d C_p^l}, \tag{8}$$

$$\dot{m}_d = \frac{dm_d}{dt} = -\frac{Sh}{3Sc} \frac{m_d}{\tau_d} \ln(1 + B_M). \tag{9}$$

In the above equations, the superscripts ‘g’ and ‘l’ refer to the gaseous state remote from the droplet location and liquid state, respectively. The latent heat of evaporation is L_v , and the gas and liquid specific heats are C_p^g and C_p^l , respectively. Further, the non-dimensional numbers for heat and mass transfer between the droplet and surrounding gas phase, and Nusselt (Nu) and Sherwood (Sh) numbers for each droplet parcel may be evaluated as²⁶:

$$Nu = 2 + 0.552Re_d^{1/2}Pr^{1/3} \tag{10}$$

and $Sh = 2 + 0.552Re_d^{1/2}Sc^{1/3}$.

In the above expression, the droplet Reynolds number is given as $Re_d = \rho_g D_d |u_d^g - v_d| / \mu_g$. The Prandtl number $Pr = \mu_g C_p^g / \lambda_g$ and the Schmidt number $Sc = \mu_g / (\rho D)_g$ are evaluated using a suitable ‘film’ composition and temperature based on the ‘1/3 rule’³⁰, where weighted-average values of composition and temperature between the gas side of the liquid droplet and gas phase remote from the droplet surface are used to evaluate the variable thermophysical properties, e.g., the dynamic viscosity μ_g , thermal conductivity λ_g , mass diffusivity $(\rho D)_g$ and specific heat capacity of the gas C_p^g appearing in the liquid phase equations. The droplet relaxation timescale is defined as $\tau_d = \rho_l D_d^2 / (18\mu_g)$ and $f_1 = 1 + 0.15Re_d^{0.687}$ is the correction to the droplet drag coefficient²⁹. The Spalding numbers, which are considered as

the driving potential for heat and mass transfers, are given as

$$B_H = C_p^g \frac{T_d^g - T_d}{L_v} \text{ and } B_M = \frac{Y_F^s - Y_{F,d}^g}{1 - Y_F^s}, \tag{11}$$

where Y_F is the fuel vapor mass fraction. The superscript ‘s’ refers to the condition on the gas side at the droplet surface. In Eq. (11), the temperature and fuel mass fractions in the gas phase far from the droplet surface are T_d^g and $Y_{F,d}^g$, respectively. Assuming thermodynamic equilibrium between the liquid and vapor phases, Y_F^s is calculated using the Clausius–Clapeyron relation in terms of the molecular weights of the air W_{air} and fuel W_F as:

$$Y_F^s = \left[1 + \frac{W_{air}}{W_F} \left(\frac{\bar{p}(x_d)}{p_F} - 1\right)\right]^{-1}, \tag{12}$$

where the partial pressure of the fuel vapor is given as

$$p_F = \exp\left[-\frac{W_F L_v}{\mathcal{R}_u} \left(\frac{1}{T^s} - \frac{1}{T^b}\right)\right]. \tag{13}$$

In the above expressions, the gas phase temperature at the droplet surface is taken as $T_g^s = T_d$, T^b is the boiling temperature of the liquid fuel at 1 atm and \mathcal{R}_u is the universal gas constant. In Eqs. (6)–(9), the gas phase velocity (u_d^g), temperature (T_d^g) and fuel mass fraction ($Y_{F,d}^g$) are needed to evaluate the evaporation rate and the temperature rise of the droplets.

Following De and Kim¹⁴, the instantaneous gas phase velocity appearing in the droplet equations may be modeled by randomly sampling a Gaussian distribution function with a mean equal to the filtered gas phase velocity (\tilde{u}) and the variance represented by $2k_{sgs}/3$. The unresolved kinetic energy of the gas phase is obtained using an equilibrium argument: $k_{sgs} = 2\Delta C_{sgs}^{2/3} \tilde{S}_{ij} \tilde{S}_{ij}$ ¹⁴. This droplet dispersion model assumes local turbulence to be isotropic. A stochastically fluctuating value of the gas phase mixture fraction, seen by an individual droplet, is randomly sampled from the subfilter FDF of the local gas phase mixture fraction, represented by computed filtered mean and variance of mixture fraction at the droplet location. Further details on the modeling of the SGS velocity/scalar fluctuations are available in De and Kim¹⁴.

3.1 Modeling of Filtered Evaporation Source Terms

The effects of droplets on the carrier gas are included through interphase source terms in the

gas phase continuity, momentum, and scalars equations. With the ‘point-particle’ assumption, a filtered, interphase transfer source term can be obtained as:

$$\bar{\dot{S}}_{\phi}(x) = \sum_d \int_V \dot{S}_{\phi,d} \delta(x_d - y) G(x - y) dy, \quad (14)$$

where $\dot{S}_{\phi,d}$ refers to the interphase transfer term arising due to the d -th droplet located at the position x_d . The subscript $\phi = \{\rho, u_i, h\}$ corresponds to the mass, momentum and enthalpy. The summation is carried out over all the particles within the domain V . The source terms, $\dot{S}_{\gamma,d}$, due to the d -th droplet parcel in the filtered continuity, momentum, and enthalpy equations are:

$$\dot{S}_{\rho,d} = -N_d \dot{m}_d, \quad (15)$$

$$\dot{S}_{u_i,d} = -N_d \frac{d}{dt} (m v_{d,i}), \quad (16)$$

$$\dot{S}_h = -N_d \frac{d}{dt} (m c_p^l T_d), \quad (17)$$

where N_d is the number of droplets in each computational parcel.

4 Mixture Fraction-Based Presumed FDF Approach

The mixture fraction concept has been routinely used for advancing our understanding of mixing and combustion processes for non-premixed turbulent flows without a phase change and led to the development of several advanced combustion models for turbulent flows. The mixture fraction is defined as the normalized value of a conserved scalar³¹. In turbulent flows, mixture fraction at a physical location undergoes random fluctuations, but it exhibits statistics similar to those observed in non-reactive flows. In mixture fraction-based presumed FDF approaches^{14, 27, 32}, fluctuations in the gas phase reactive scalars (temperature, species mass fractions) are assumed to be associated with those in conserved scalar mixture fraction. Mean values of reactive scalars, i.e., composition and temperature at any physical location, are obtained by convoluting their instantaneous state relationship to the mixture fraction with the FDF of the mixture fraction.

4.1 Bilger’s Definition of Mixture Fraction for Reactive Sprays

Classical and current approaches^{33, 34} of the droplet and spray combustion utilize the concept of conserved scalars in the form of Shvab-Zel’dovich

variables. In most of the previous modeling effort on turbulent spray combustion^{32, 35}, the conventional definition of mixture fraction has been routinely used, which remains conserved within the pure gaseous phase. Such a mixture fraction no longer remains a conserved quantity in the presence of evaporating droplets. Naturally, there exists a disjoint between the treatment of the droplet evaporation with the established theory and modeling of non-premixed mixing and combustion processes in the gas phase³⁶. As a result, the same conserved scalar could not be used to describe the aforementioned liquid and gas phase phenomena. Bilger³⁶ provides seamless integration of treatment of the droplet evaporation and modeling of mixing and combustion processes in the gas phase by defining the mixture fraction that is valid in both the gas and the liquid phases instantaneously. In LES, only the filtered quantities of the instantaneous flow field variables, namely velocity, temperature, and composition, are resolved. As a consequence, if the liquid phase-governing equations are solved using these filtered gas phase variables, then the effect of the subgrid-scale fluctuations would not be considered. Therefore, the inclusion of the effect of these SGS fluctuations becomes necessary to accurately describe the droplet dispersion and interphase heat/mass transfer rates. In most of the previous studies, the liquid phase-governing equations are very often solved by assuming that the gas phase properties seen by droplets are typically taken as the filtered values, and thereby neglecting the subgrid fluctuations in gas phase reactive scalars, namely, temperature and composition. Neglecting the scalar fluctuations may not be justified in reacting sprays, as it is well known that there exist strong effects of turbulent mixing on fluctuations in gas phase reactive scalars. Bilger’s definition of mixture fraction has been used in the context of RANS-based fully stochastic separated flow (FSSF) approach of turbulent reacting sprays¹³. Following Bilger³⁶, the mixture fraction is defined as unity and zero in liquid droplet and pure gas phases, respectively. Turbulence-chemistry interaction is modeled using a presumed PDF of the mixture fraction with infinite fast chemistry assumption within the gas phase represented by a single-step irreversible reaction.

4.2 Flamelet Progress Variable Approach

The flamelet progress variable (FPV) model was originally proposed by Pierce and Moin³⁷ for non-premixed gaseous phase combustion in the context of LES. The FPV approach successfully

predicted extinction/re-ignition phenomena in non-premixed turbulent flames³⁸. The mixture fraction-based RANS-FSSF model¹³ has been extended to LES of reacting sprays where the finite-rate gas phase chemistry is considered via flamelet progress variable (FPV) approach¹⁴, where a novel stochastic method is proposed to consider the effects of the SGS fluctuations of the gas phase reactive scalars on droplet evaporation and interphase heat/mass transfer. The effects of the subgrid evaporating droplets on the modeling of the two-phase source terms in the transport equation of variance of mixture fraction, subfilter scalar mixing processes and subfilter fluctuations in the gas phase reactive scalars on droplet evaporation and dispersion are modelled.

In the FPV approach, the internal structure of turbulent flame is assumed to remain laminar⁵, and a reactive scalar is defined using the computed flamelet solution. The flamelet equations are solved to obtain the state relationship or mapping between a reactive scalar (or chemical source term) and reference space or independent variables, namely, mixture fraction Z and reaction progress variable, C ³⁹. The progress variable is usually defined as the sum of product mass fractions, $C = Y_{H_2} + Y_{H_2O} + Y_{CO} + Y_{CO_2}$ ^{14, 27}. Several other definitions of progress variable are possible. In FPV, the filtered reactive scalars are obtained by convoluting $\phi(Z, C)$ with the joint FDF of the mixture fraction and the progress variable $\tilde{P}(Z, C)$. The joint FDF may be approximated as $\tilde{P}(Z, C) = \tilde{P}(C)\tilde{P}(Z)$ by assuming Z and C to be statistically independent. The β -function is used often to represent $\tilde{P}(Z)$ ^{9, 14, 27}. For $\tilde{P}(C)$, Dirac delta function, $\delta(C - \tilde{C})$, as used to approximate $\tilde{P}(C)$ ^{13, 37}. A β -function for reaction progress variable may also be used as done in the LES—flamelet generated manifolds (FGM) study^{40, 41}. For the dilute spray regime, the standard β -function parameterized by the filtered mean and the subgrid variance of the mixture fraction is used for the FDF of the mixture fraction, $\tilde{P}(Z)$, with $0 \leq Z \leq 1$ ^{9, 14}. In FPV, additional transport equations for the filtered mixture fraction, subgrid variance of mixture fraction and filtered reaction progress variable \tilde{C} are solved. The filtered equations for the mixture fraction and reaction progress variable are obtained by employing phase-conditional filtering and invoking ‘dilute spray’ assumption³⁶:

$$\frac{\partial(\bar{\rho}\tilde{C})}{\partial t} + \frac{\partial(\bar{\rho}\tilde{u}_j\tilde{C})}{\partial x_j} = \frac{\partial}{\partial x_j} \left(\bar{\rho}\tilde{D} \frac{\partial\tilde{C}}{\partial x_j} \right) - \frac{\partial q_{j,C}^{sgs}}{\partial x_j} + \bar{\rho}\tilde{\omega}_C, \tag{18}$$

$$\frac{\partial(\bar{\rho}\tilde{Z})}{\partial t} + \frac{\partial(\bar{\rho}\tilde{u}_j\tilde{Z})}{\partial x_j} = \frac{\partial}{\partial x_j} \left(\bar{\rho}\tilde{D} \frac{\partial\tilde{Z}}{\partial x_j} \right) - \frac{\partial q_{j,Z}^{sgs}}{\partial x_j} + \bar{\rho}\tilde{\omega}_Z, \tag{19}$$

$$\begin{aligned} \frac{\partial(\bar{\rho}\tilde{Z}''^2)}{\partial t} + \frac{\partial(\bar{\rho}\tilde{u}_j\tilde{Z}''^2)}{\partial x_j} &= \frac{\partial}{\partial x_j} \left(\bar{\rho}\tilde{D} \frac{\partial\tilde{Z}''^2}{\partial x_j} \right) \\ &- \frac{\partial q_{j,Z''^2}^{sgs}}{\partial x_j} + 2\bar{\rho}\mathcal{D}_{t,Z} \left(\frac{\partial\tilde{Z}}{\partial x_j} \right)^2 - \bar{\rho}\tilde{s}_{\chi Z} + \tilde{S}_{Z''^2}, \end{aligned} \tag{20}$$

where \mathcal{D} is the molecular diffusivity. In the above transport equations, the SGS scalar fluxes $q_{j,\phi}^{sgs}$ where, $\phi = \{Z, Z''^2, C\}$, are modeled as follows:

$$q_{j,\phi}^{sgs} = \bar{\rho}\tilde{u}_j\tilde{\phi} - \bar{\rho}\tilde{u}_j\tilde{\phi} = -\bar{\rho}\mathcal{D}_{t,\phi} \frac{\partial\tilde{\phi}}{\partial x_j}. \tag{21}$$

The dynamic model²² may be used to determine the turbulent diffusivity, $\mathcal{D}_{t,\phi} = C_{sgs,\phi} \Delta^2 |\tilde{S}_{ij}|$. The constant $C_{sgs,\phi}$ is determined separately for each variable $\phi = \{Z, Z''^2, C\}$ at all physical locations. The chemical source term, $\tilde{\omega}_C$ in Eq. (18), is obtained after convoluting $\tilde{\omega}_C(Z, C)$ with the joint FDF $\tilde{P}(Z, C)$ as discussed earlier. The subgrid scalar dissipation rate $\tilde{s}_{\chi Z}$ term appearing in Eq. (20) is modeled assuming a linear relaxation for the SGS scalar dissipation rate, $\tilde{s}_{\chi Z} = \frac{Z''^2}{\tau_\phi}$. Here, the scalar mixing timescale is $\tau_\phi = \frac{\tau_t}{C_\phi}$, turbulent SGS timescale is $\tau_t \approx \Delta^2 / \max(\mathcal{D}, \mathcal{D}_t)$ and C_ϕ is the scalar dissipation constant. For gaseous mixing, $C_\phi = 2$ is widely used, while higher values have also been reported using the transported FDF simulations^{42, 43}. Evaporating droplets are expected to significantly affect the small-scale mixing process. However, a thorough understanding of their effects on the scalar dissipation rate is lacking. The last terms in Eqs. (18)–(19) are the source terms due to interphase transfer. The evaporation source terms in Eqs. (8)–(9) may be written as^{36, 44}:

$$\tilde{S}_Z = \tilde{S}_\rho \text{ and } \tilde{S}_{Z''^2} = \overline{(2Z - Z^2)\tilde{S}_Z} - \tilde{Z}(2 - \tilde{Z})\tilde{S}_Z. \tag{22}$$

More details on the evaluation of the interphase transfer terms are available in De and Kim¹⁴. This approach simplifies the construction of the flamelet lookup table used in LES, since the parameter Z^s (Eq. (17)) does not need to be considered. However, there are instances when a modified form of the β -function between $Z = 0$ and the local maximum mixture fraction of the

gas phase $Z = Z_m$ are used following the conventional definition of mixture fraction. The effect of radiation could be included in flamelet models by introducing another parameter, namely, enthalpy defect, which represents a departure from the adiabatic condition^{27, 45}. Most state-of-the-art research that accounts for the flamelet library generation for non-adiabatic processes have only dealt with radiation for pure gas phase combustion⁴⁶. The modeling of these non-adiabatic processes remains an open problem since the spray distribution in the physical space is entirely uncorrelated to the mixture fraction space.

4.3 Conditional Moment Closure Method

In non-premixed flows, where there is mixing between fuel and oxidizer streams, the reactive scalars within the mixing field depend strongly on the local and instantaneous value of the mixture fraction $Z(x, t)$. The conditional expectation $Q(\eta; x, t)$ of a scalar variable $\phi(x, t)$, conditioned on the associated value $Z(x, t)$ taking a specific value η is defined as $Q(\eta; x, t) = \overline{\phi(x, t) | Z(x, t) = \eta}$. Here, the notation of vertical bar indicates that the average is taken upon those members of the ensemble which obey the condition to the right of the bar. Then, the local and instantaneous value of the scalar can be decomposed as: $\phi(x, t) = Q[Z(x, t); x, t] + \phi''(x, t)$. In the conditional moment closure (CMC) method^{6, 7}, the transport equations for conditional scalars (temperature or enthalpy and species conservation) may be derived either from the joint-FDF method or decomposition method. The CMC equations are derived based on the assumption that most of the fluctuations in scalar quantities of interest could often be associated with the fluctuation of one key quantity. If closure of the conditional scalars appearing in the reaction rate term is achieved at the first-moment level by neglecting the conditional fluctuations, the model is said to be 'first-order CMC' model. The transport equation of the conditional moment of any species α may be written as in^{47, 48}:

$$\begin{aligned} \frac{\partial}{\partial t} Q_\alpha + \frac{1}{\bar{\rho}_\eta \tilde{P}_\eta} \nabla \cdot \left[\bar{\rho}_\eta \tilde{P}_\eta (u_\eta Q_\alpha - \mathcal{D}_{t,\eta} \nabla Q_\alpha) \right] \\ = \bar{\omega}_{\eta,\alpha} + N_\eta \frac{\partial^2 Q_\alpha}{\partial \eta^2} + \frac{Q_\alpha}{\bar{\rho}_\eta \tilde{P}_\eta} \nabla \cdot \left(\bar{\rho}_\eta \tilde{P}_\eta u_\eta \right). \end{aligned} \quad (23)$$

Here, the subscript η denotes the conditionally averaged property, N_η the scalar dissipation rate and u_η is the conditional velocity. The conditional

reaction rate, $\bar{\omega}_{\eta,\alpha}$ in first-order CMC model with single-step reaction is directly obtained from the Arrhenius reaction rate expression using conditional mean values of temperature and composition^{44, 49}. For cases where the fluctuations about conditional means of a scalar are present in significant proportions (e.g., flames with extinction and re-ignition), the closure is necessary at the second moment level, which is known as 'second-order CMC' model⁵⁰. Sometimes, another variable such as sensible enthalpy is used as the second conditioning variable⁵¹. The CMC equations with added dimension (mixture fraction space) are solved in tandem with flow field in case of fully coupled equations. The flow solver provides the mixing field information to the CMC equations, while the CMC solver offers the data of the mean density field to the flow solver. However, the CMC model incurs tremendous computational efforts mainly due to the added dimension, namely the mixture fraction space.

5 Transported FDF Method

Transported PDF (TPDF) methods for reactive flows were introduced initially in the context of RANS¹⁰. Later, the application of this method was extended to LES based on the concept of FDF^{11, 52–54}. In the transported FDF (TFDF) method, the turbulent field is described by the transport equation of joint FDF of the velocity and scalars (enthalpy and species mass fractions). The transport equation of joint FDF may be derived from Navier–Stokes equations and conservation equations for scalars^{12, 55}. Only very few attempts have been made so far on the TFDF method for turbulent reactive flows with phase change^{16, 56–58}. In the following section, we briefly present the composition FDF transport equation, followed by Lagrangian particle and Eulerian stochastic fields (ESF) solution approaches.

5.1 Transport Equation of Composition FDF

The filtered scalars may be obtained using the one-point, one-time joint FDF of the continuous gas phase: $\tilde{P}(\psi; x, t)$ ¹⁶, where ψ is the sample space variable corresponding to the composition vector $\{\phi_\beta, h; 1 \leq \beta \leq N\}$ containing species mass fractions (N) and enthalpy, respectively. The joint FDF may be defined as^{11, 52, 57, 59},

$$\tilde{P}(\psi; x, t) = \int \delta[\psi, \phi(y, t)] G(x - y) dy, \quad (24)$$

where δ is the Dirac delta function. The filtered density, $\bar{\rho}$, may be obtained in terms of the joint FDF as $\bar{\rho}(x, t) = \int \tilde{P}(\psi; x, t) d\psi$. The term

$\varrho[\psi, \phi(x, t)] = \delta[\psi - \phi(x, t)] = \prod_{\alpha=1}^{N_s} \delta[\psi_\alpha - \phi_\alpha(x, t)]$ is the fine-grained density (ϱ)^{11, 52, 60}, where $N_s = N + 1$ is the total number of reactive scalars (N , enthalpy), i.e., $\{\phi_\beta, h; 1 \leq \beta \leq N, 1 \leq \alpha \leq N_s\}$. The transported FDF equation may be written as^{16, 57}

$$\begin{aligned} & \frac{\partial \tilde{P}}{\partial t} + \frac{\partial \tilde{u}_i \tilde{P}}{\partial x_i} - \frac{\partial}{\partial x_i} \left(\tilde{\rho} \mathcal{D}_t \frac{\partial \left(\frac{\tilde{P}}{\tilde{\rho}} \right)}{\partial x_i} \right) \\ &= - \sum_{\beta=1}^N \frac{\partial}{\partial \psi_\beta} \left[\widetilde{\mathcal{D}_\beta | \psi} + \tilde{\omega}_\beta(\psi) + (\phi_\beta^f - \psi_\beta) \widetilde{\dot{S}_\rho | \psi} \right] \tilde{P} \\ & \quad - \frac{\partial}{\partial \psi_h} \left[\widetilde{\mathcal{D}_h | \psi} + \tilde{\omega}_h(\psi) + (\dot{S}_h | \psi - \psi_h \widetilde{\dot{S}_\rho | \psi}) \right] \tilde{P} \\ & \quad + \widetilde{\dot{S}_\rho | \psi} \tilde{P}. \end{aligned} \tag{25}$$

In the above equation, \mathcal{D}_t is turbulent diffusivity, ϕ_β^f is the mass fraction of any specie ‘ β ’ in the evaporating spray droplet, $\tilde{\omega}_h(\psi)$ is the source term in the energy equation due to chemical reactions and $\mathcal{D} = \frac{1}{\tilde{\rho}} \frac{\partial}{\partial x_i} \tilde{\rho} \mathcal{D} \frac{\partial \phi_\alpha}{\partial x_i}$ is the diffusion term. The contributions arising due to evaporating droplets are modeled by the conditional evaporation rate source term $\widetilde{\dot{S}_\rho | \psi}$, and the source term due to energy interactions between the gas and liquid phase $\widetilde{\dot{S}_h | \psi}$. The salient feature of the transported PDF/FDF methods is that the chemical source term $\tilde{\omega}_\alpha(\psi)$ appears as closed and requires no modeling. However, the molecular mixing or micro-mixing term in the reactive scalar space, the fluctuating pressure term and the transport of FDF in the velocity space by viscous stresses require closure models. The micro-mixing term may be closed using various molecular mixing models, such as the Euclidean minimum spanning tree (EMST)⁶¹, interaction by exchange with mean (IEM) or linear mean square estimation (LMSE)^{52, 62} and the modified curl (MC)⁶¹ models. Heye et al.^{16, 57} used the IEM model to close the conditional subgrid diffusion terms as

$$\widetilde{\mathcal{D}_\beta | \psi} = \frac{1}{\tau_\phi} (\psi_\beta - \tilde{\phi}_\beta), \tag{26}$$

$$\widetilde{\mathcal{D}_h | \psi} = \frac{1}{\tau_\phi} (\psi_h - \tilde{h}). \tag{27}$$

The solution of transported PDF/FDF equation becomes infeasible using conventional numerical methods, as the computational cost increases exponentially with an increase in the number of scalars used to describe the joint FDF $\tilde{P}(\psi; x, t)$. Monte Carlo (MC) method using Lagrangian particles^{52, 63–65} and Eulerian stochastic fields (ESF) method^{16, 57, 66, 67} are often used to achieve a solution of the joint FDF equation.

5.2 Lagrangian Particle Method

In this approach^{16, 59, 63}, the transport equation of FDF, Eq. (25) is converted to equivalent stochastic differential equations (SDE) and solved using an ensemble of notional particles, which evolve in time and space based on the Lagrangian framework by solving the SDEs. Individual notional particles carry fluid properties, such as weight w_i , position x_i , composition ϕ_i and enthalpy h_i . The sum of weights of all particles is equal to the gas phase density at that location, i.e., $\sum_{i=1}^{N_p} w_i = \tilde{\rho} \Delta_v$, where Δ_v is the filter volume and N_p is the number of stochastic particles in that volume.

Using the MC method, the SDEs are solved to evolve the fluid property vector in the physical and the composition spaces¹⁶. The transport of the particles in the physical space may be described as^{52, 63}:

$$\begin{aligned} dx_i &= \left[\tilde{u}_i + \frac{1}{\tilde{\rho}} \frac{\partial}{\partial x_i} \tilde{\rho} (\mathcal{D} + \mathcal{D}_t) \right] \Delta t \\ & \quad + \sqrt{2(\mathcal{D} + \mathcal{D}_t)} d\omega_i, \end{aligned} \tag{28}$$

where Δt is the time step, and $d\omega_i$ is the Weiner term in the i -th direction. The change in particle composition may be written as

$$d\phi_\alpha = \frac{1}{\tau_\phi} (\phi_\alpha - \tilde{\phi}_\alpha) \Delta t + \dot{\omega}(\phi_\alpha) \Delta t. \tag{29}$$

After the solution of the SDE, the filtered value of any scalar ϕ is obtained in terms of the weighted average as $\tilde{\phi}_\alpha = \frac{\sum_{j=1}^{N_p} w_j \phi_\alpha}{\sum_{j=1}^{N_p} w_j}$. Though the Lagrangian MC method is more accurate than the ESF method, it becomes computationally intensive with an increase in the number of notional particles⁶⁸.

5.3 Eulerian Stochastic Fields Approach

In the ESF approach, the transport equation of FDF, Eq. (26) is solved by representing $\tilde{P}(\psi; x, t)$ as an ensemble of N_{sf} notional stochastic fields⁶⁷. A system of SDEs is solved to describe the evolution of each stochastic field for all CFD cells within the Eulerian framework. In the ESF model, the joint FDF $\tilde{P}(\psi; x, t)$ is represented by N_{sf} stochastic fields $\xi_\alpha^k(x, t); 1 \leq k \leq N_{sf}, 1 \leq \alpha \leq N_s$ for all N_s ($N + 1$) scalar variables $\{\phi_\beta, h; 1 \leq \beta \leq N\}$ ⁶⁹:

$$\begin{aligned} \tilde{P}(\psi; x, t) &= \frac{1}{\tilde{\rho} N_{sf}} \sum_{k=1}^{N_{sf}} \int \rho G(x - y) dy \\ & \quad \times \prod_{\alpha=1}^{N_s} \delta[\psi_\alpha - \xi_\alpha^k(x, t)]. \end{aligned} \tag{30}$$

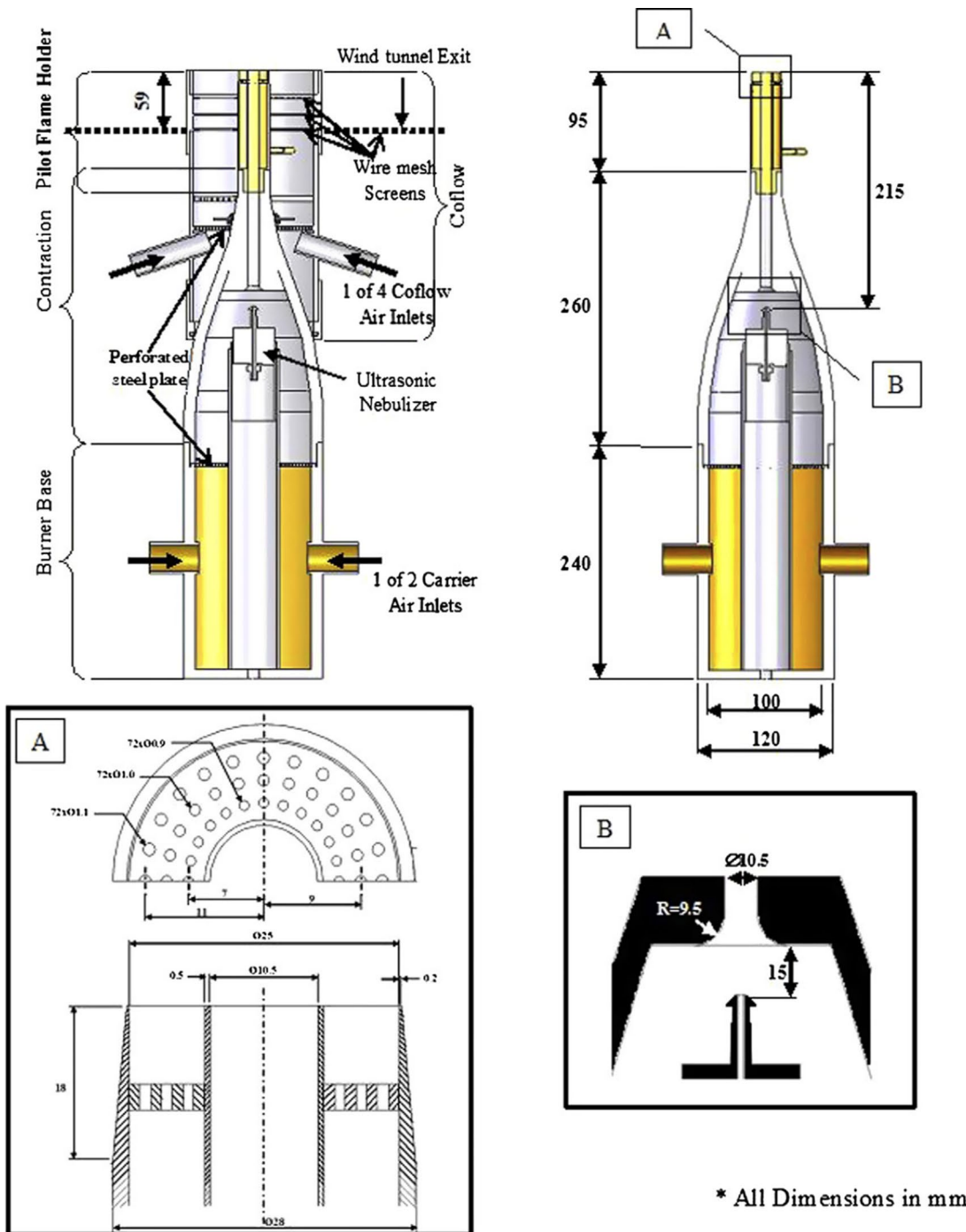


Figure 1: Experimental dilute spray burner of Gounder and Masri^{71, 72}.

The system of SDE governing the evolution of these stochastic fields $\xi_{\alpha}^k(x, t)$ may be derived following Ito⁶⁷ or Stratonovich⁷⁰ formulation. The mean value of the reactive scalars is obtained by averaging the stochastic fields as $\bar{\phi}_{\alpha} = \frac{1}{N_{sf}} \sum_1^{N_{sf}} \xi_{\alpha}^k$.

6 Recent Numerical Simulations of Spray Combustion

In this section, the gas- and liquid-phase statistics are presented from recent numerical simulations using different turbulent combustion models for dilute reactive sprays. As mentioned earlier, development and validation of computational models for turbulent spray combustion

require well-defined inlet boundary conditions and measurements at downstream locations. Here, we present limited numerical results on reactive spray burners at the University of Sydney¹⁸. Two different spray burners are chosen, namely piloted spray jet flame burner of Gounder and Masri^{19, 71, 72} and auto-igniting spray flames stabilized by vitiated co-flow of O'Loughlin and Masri^{20, 73}. The turbulent spray combustion database of the University of Sydney has been popular among the modelers due to availability of well-defined inlet boundary conditions and measurements at several downstream locations. Different fuels, e.g., acetone, ethanol and methanol were used in experiments. Apart from the Sydney spray flames, some other configurations have been used recently for dilute spray flames, among which Cambridge spray burner⁷⁴, burner of Karpetis and Gomez⁷⁵, CORIA Rouen burner^{76–78} and Delft spray in hot co-flow^{79, 80} offer well-defined measurements for validation of numerical models. A list of the recent database on spray flames is available in Jenny et al.¹

The Sydney piloted spray burner^{19, 71, 72}, as shown in Fig. 1, employed an ultrasonic nebulizer

to produce liquid droplets, which get entrained by the carrier air 215 mm upstream of the jet exit. The atomized fuel is carried by a stream of carrier air. Surrounding the jet and pilot is an air co-flow which shrouds the flame from the ambient air. De et al.¹³ studied numerically the ethanol reacting spray flames^{19, 71, 72} using the FSSF approach with fast chemistry assumption (discussed in Sect. 4.1) for the gas phase. The flames studied were EtF1, EtF4 and EtF7 ('Et' meaning ethanol fuel, 'F' for flame) and the succeeding numbers represent conditions at the jet exit, such as equivalence ratio ϕ_{eq} and carrier air velocity. EtF7 has the highest jet velocity among all flames of the EtF series. Also, Et7 has the lowest amount of evaporated fuel at the jet exit with an equivalence ratio of $\phi_{eq,exit} = 0.05$ at the jet exit, followed by EtF4 and EtF1 having $\phi_{eq,exit} = 0.53$ and 1.75, respectively.

Radial profiles of the filtered gas phase temperature are shown in Fig. 2. A comparison is made between the prediction capabilities of two RANS-based models, namely, FSSF and the conventional stochastic separated flow (CSSF) model. It is seen that the FSSF model yields a better agreement with the experiments compared to

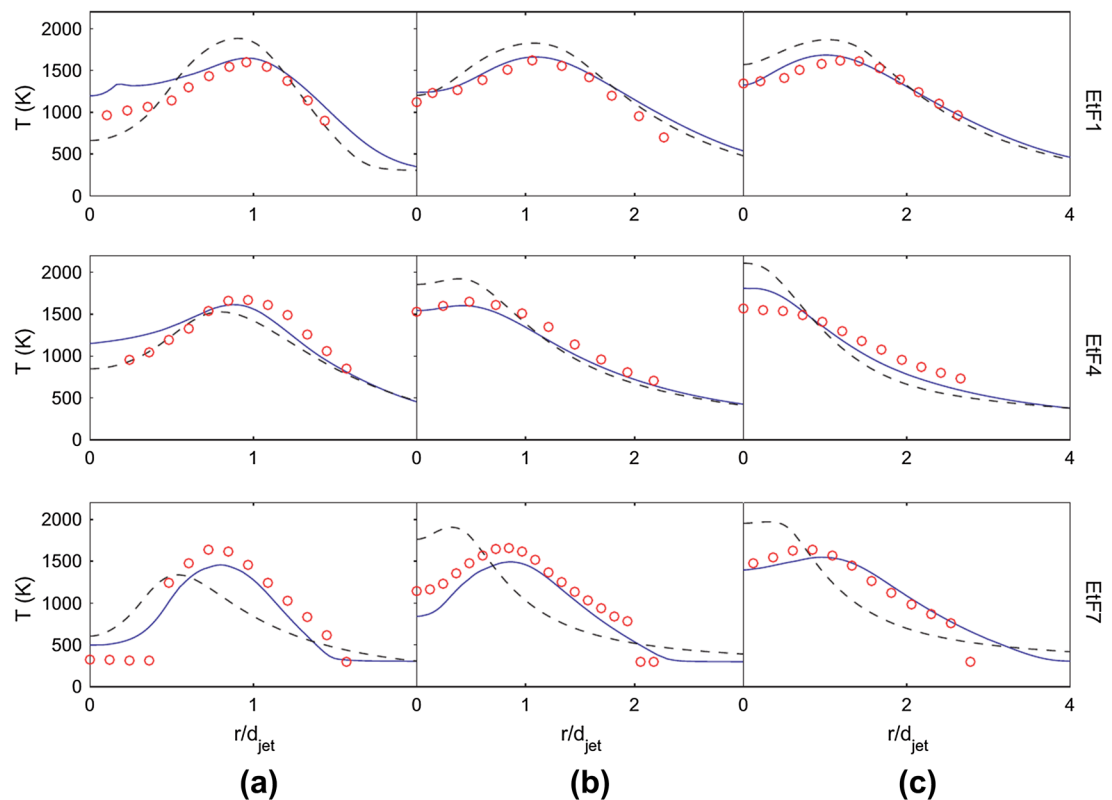


Figure 2: Radial profiles of filtered mean temperature for the flames EtF1, EtF4 and EtF7 at axial locations: **a** $x/D=10$, **b** $x/D=20$, and **c** $x/D=30$. Solid line, FSSF model¹³, dashed line, CSSF model¹³, and symbols, experimental data⁷².

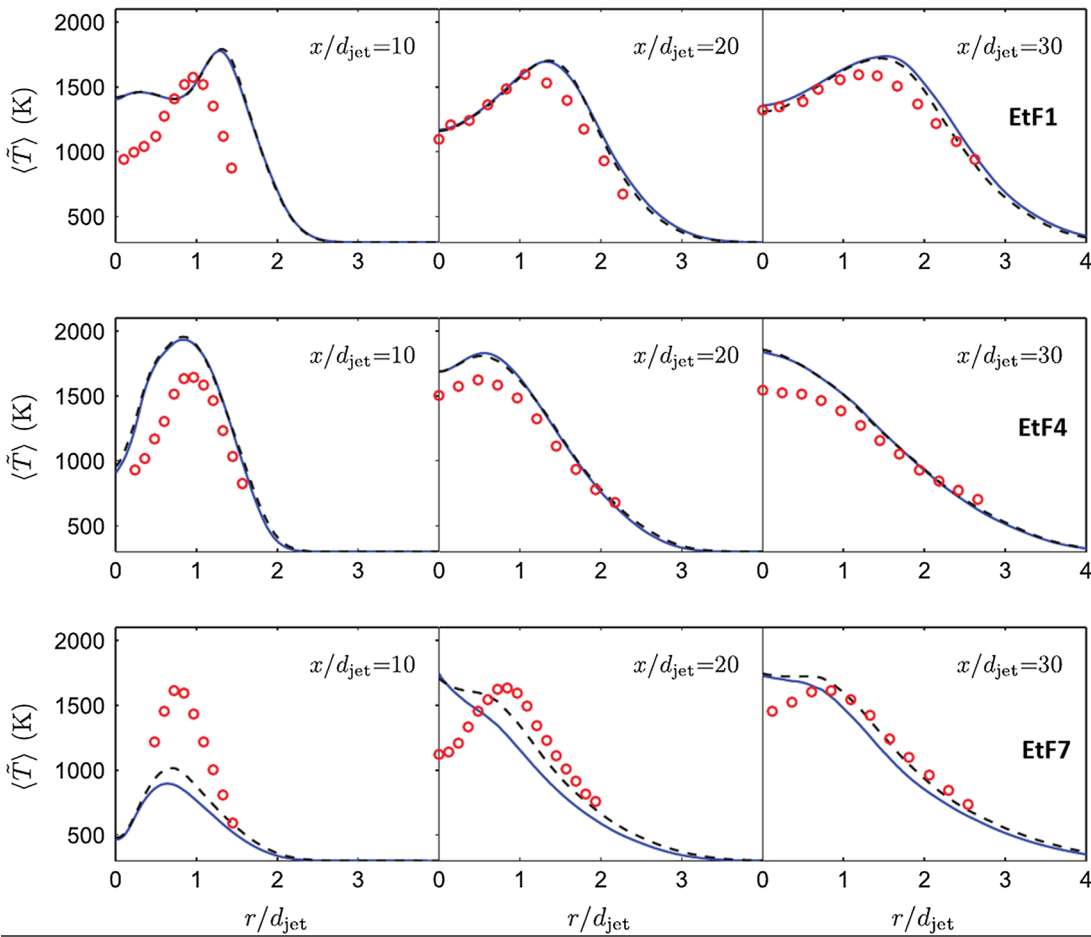


Figure 3: Radial profiles of gas phase mean temperature [¹⁴] with dashed lines-NF-E3, solid lines-SF-E3 and (circle)-experimental data [¹⁴].

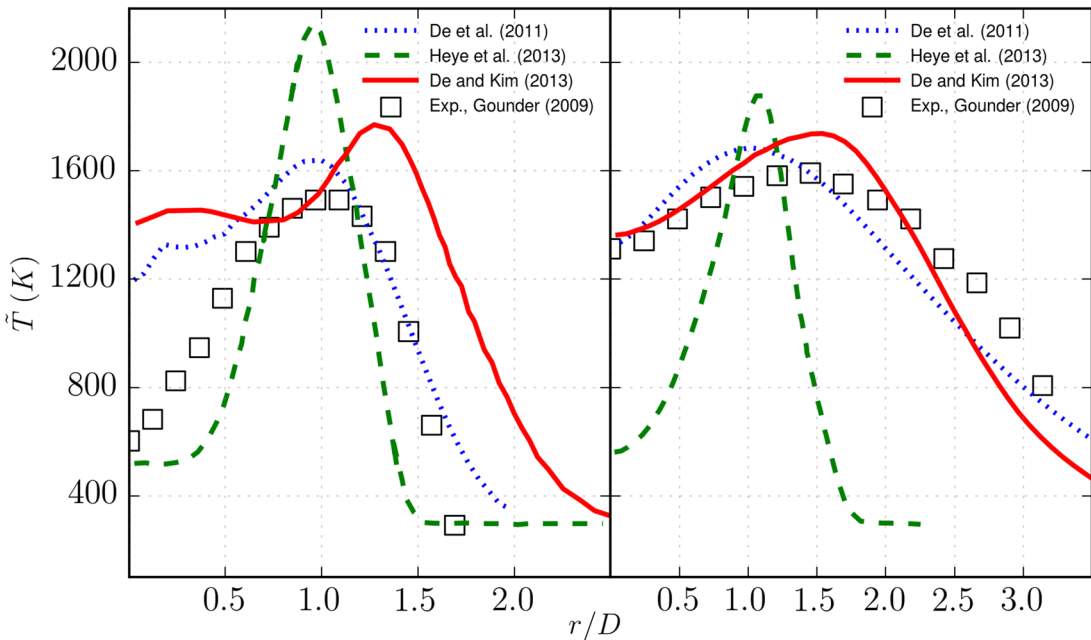


Figure 4: Radial profiles of time-averaged temperature for EtF1 from RANS-FSSF approach of De et al.¹³ LES-FPV of De and Kim¹⁴ transported FDF approach of Heye et al.¹⁶ and experimental data of Gounder¹⁰ at $x/D = 10$ (left) and $x/D = 30$ (right).

the CSSF model. Considering the experimental uncertainties being as high as 10%¹³, the choice of the modeling approach appears to be convincing. De and Kim¹⁴ applied the LES-FPV approach (see Sect. 4.2) to study these flames mentioned above, namely EtF1, EtF4 and EtF7. The predicted Favre mean temperature profiles are shown in Fig. 3 from two different simulations with different subgrid-scale mixing and evaporation models, namely SF-E3 (subgrid scalar fluctuation for droplet and transport equation for Z''^2 with $C_\phi = 8$) and NF-E3 (no subgrid scalar fluctuation and transport equation for Z''^2 -Eqn. with $C_\phi = 8$). Inclusion of the SGS scalar fluctuations does not improve the temperature predictions for EtF1 and EtF4 but lead to an underprediction of temperature for EtF7. Overall, the results appear to be in reasonable agreement except for the case with a low amount of pre-evaporated fuel at the jet exit (EtF7).

Heye et al.¹⁶ performed simulations of the EtF1 flame using the Lagrangian particle method (see Sect. 5.2), where the joint FDF of the mixture fraction (Z) and reaction progress variable (C) is solved. The radial profiles of time-averaged, filtered temperature are shown in Fig. 4 at two axial locations, and numerical results are compared with the available experimental measurements. An average of 20 notional particles per computational cell was used during these simulations.

A separate simulation of turbulent flow in a pipe is used to prescribe the inflow turbulence flow field for the gas phase. As may be seen in Fig. 4, the spreading of the jet is very slow when compared to the experiments. The simulations do not predict the temperature distribution within the flame, which the authors attributed to the lack of precise inflow conditions. For a comparison, temperature profiles from RANS-FSSF¹³, LES-FPV¹⁴ and transported FDF model¹⁶ are shown in Fig. 4.

There is no prediction from the CMC model (see Sect. 4.3) for the EtF flames. The CMC has been used to simulate acetone spray flames of Gounder and Masri^{71, 72}. Only a few studies of CMC applied to spray flames are available in the literature. Here, we present numerical results from the CMC model of Ukai et al.³² for the acetone spray flame AcF3. Apart from this, CMC with tabulated chemistry⁸¹ and the CMC method based on two conditional moments¹⁵ are also available in the literature. Ukai et al.³² used artificial inflow turbulence using the digital filtering techniques of Klein et al.⁸² and simulated the acetone spray flames, which are similar to the ethanol spray flames mentioned above with difference being the equivalence ratio at the jet exit ($\phi_{\text{e,exit}}$). Two meshes, $96 \times 96 \times 240$ and $3 \times 3 \times 40$, were used, respectively, for solving LES and CMC equations, respectively³². Radial profiles of the time-averaged filtered temperature

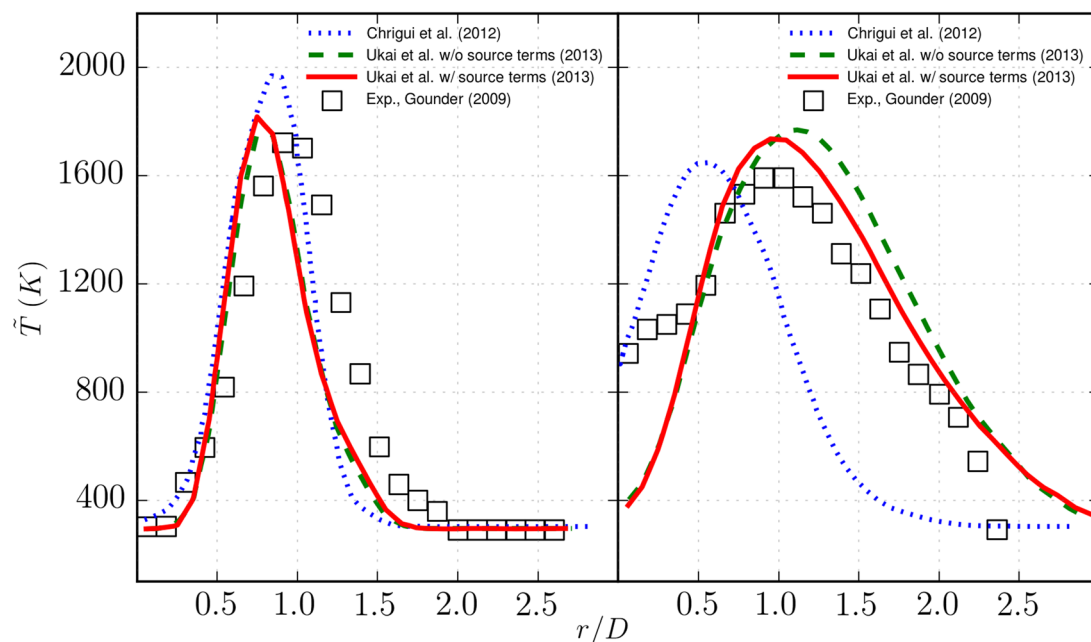


Figure 5: Radial profiles of average temperature for the AcF3 from LES-FGM of Chrigui et al.³⁷, CMC method of Ukai et al.³² with and without spray source terms in the CMC equations and experimental measurements of Gounder¹⁹ at $x/D = 10$ (left) and $x/D = 30$ (right).

from the CMC model³² and LES-FGM of Chrigui et al.²⁷ are plotted in Fig. 5 at two axial locations, $x/D=10$ and 30. Further, a comparison of the predicted temperature profile with and without the spray evaporation source terms in the CMC equations are also shown in Fig. 5. The trend of predicted filtered mean temperature agrees well for both the methods. At $x/D=30$, it is seen that the inclusion of the spray evaporation source terms yields a better agreement in the prediction of flame temperature. Both models underpredict the centerline temperature at $x/D=30$, which may be attributed to measurement errors using thermocouples and poor choice of inflow conditions. Overall, a reasonable agreement is achieved by these two techniques, which was further improved using the CMC method with tabulated chemistry⁸¹ and by solving two conditional moments¹⁵.

Besides the Sydney pilot-stabilized spray burner, the Sydney auto-igniting spray burner has also been used toward validation of turbulent combustion models. Among numerical studies on this burner, we present results from transported FDF methods, namely Lagrangian particle method (see Sect. 5.2) of Heye et al.⁵⁷ and ESF method (see Sect. 5.3) of Prasad et al.⁸³. The autoigniting spray in hot co-flow burner has a central jet, surrounded by a co-flowing oxidizer stream consisting of hot combustion products

from a lean premixed hydrogen/air flame stabilized over a perforated annular burner. The spray is produced by an ultrasonic atomizer, and the liquid droplets are entrained by ambient air (or inert nitrogen) stream. Further details on this spray burner may be found in Refs.^{20, 73}. Comparison of the Favre filtered mean temperature is shown in Fig. 6 for the Mt2A spray flame from the Lagrangian particle method⁵⁷ and ESF method⁸³. The Mt2A case has 1.8% of pre-evaporated methanol at the jet exit. In the Lagrangian particle method, detailed chemical kinetics is used based on in situ adaptive tabulation (ISAT)⁸⁴ technique, where an average of 20 notional particles per computational cell is used. As seen in Fig. 6, both approaches could reasonably predict the trend in temperature observed during the experiment. Prasad et al.⁸³ carried out a sensitivity study using $N_{sf} = 1$ and $N_{sf} = 8$ for the Mt2A case. At $x/D=5$, the predicted temperature profile is somewhat insensitive to the number of stochastic fields; however, further downstream, at $x/D=40$, a noticeable variation in the temperature is observed with the number of stochastic fields employed. It can be seen that the calculations using $N_{sf} = 8$ are closer to the experimental predictions than those obtained using $N_{sf} = 1$.

One of the advantages of the Sydney spray burners^{18–20} is the availability of the detailed measurements of liquid phase statistics, such as mean

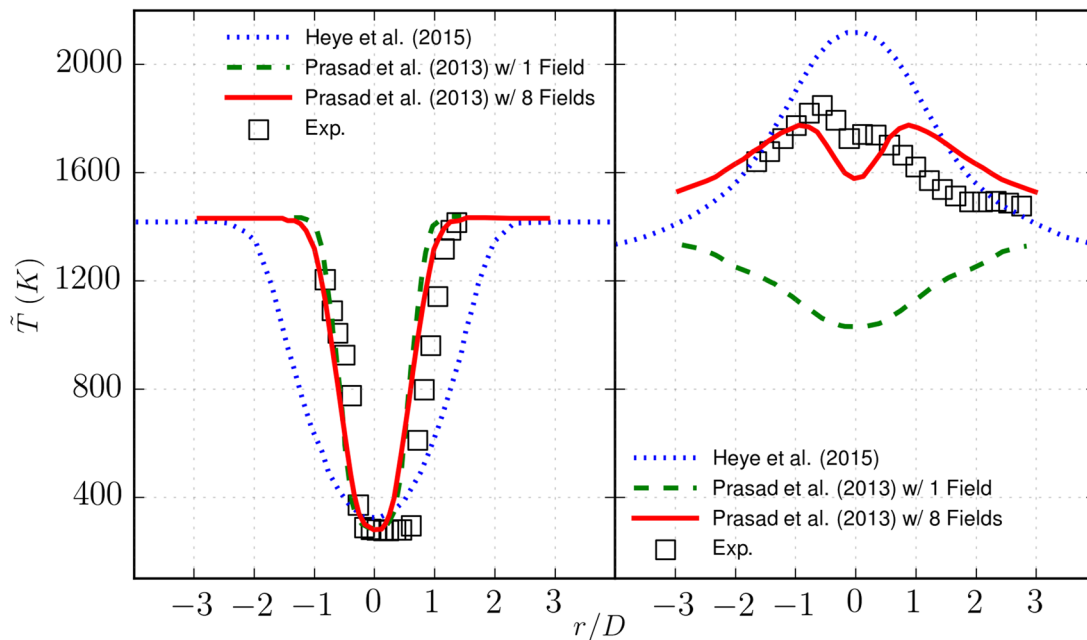


Figure 6: Mean temperature of gas phase for the Mt2A from Lagrangian MC model of Heye et al.⁵⁷, TFDF solution with one and eight stochastic fields of Prasad et al.⁸³ and experimental results of O'Loughlin^{20, 73} at $x/D=5$ (left) and $x/D=40$ (right).

and rms velocity, Sauter mean diameter (SMD) for different size classes of liquid droplets at several downstream locations, which is extremely helpful toward model development and validation. In the present article, we do not attempt to present liquid phase statistics. Needless to say, most of the models for turbulent combustion described above could reasonably predict the liquid phase statistics.

7 Conclusions

A brief overview of the numerical models for turbulent spray combustion is presented with results from recent numerical studies performed using the experimental measurements of the University of Sydney^{18–20}. In this review article, we present state-of-the-art turbulent combustion models for gaseous phase which have been extended to simulate dilute spray combustion. No attempt has been made to provide information on complex physical processes involving atomization, secondary breakup, particle-particle interactions, particle-wall interactions and modeling of dense sprays. While presenting the recent numerical results, we consider two popular spray combustion burners, namely Sydney piloted spray burner and Sydney spray in a hot vitiated co-flow burner. These dilute spray burners with well-defined inlet boundary conditions are suitable for the development and validation of the numerical models for turbulent spray combustion. Most turbulent combustion models when extended to spray combustion could capture the experimental trend; however, differences in numerical results are noticed in regions with high droplet mass loading. Some significant conclusions on different turbulent spray combustion models and possible future research directions are provided below:

1. RANS-based infinitely fast chemistry approach used by De et al.¹⁷ reasonably predicts the EtF flame series⁴³, but may seem inappropriate for applications requiring detailed species predictions.
2. LES-based flamelet models seem to predict the overall flame structure of spray flames reasonably. However, there is a mismatch in regions with high droplet mass loading. Further, the flamelet model cannot capture transient combustion phenomena, such as extinction and re-ignition, adequately.
3. The CMC method has been recently applied to model turbulent spray flames, which can capture the transient combustion phenomena to some extent. However, the CMC

method becomes computationally prohibitive when the number of species increases.

4. LES-based transported FDF approaches are regime independent and can predict extinction and re-ignition phenomena with reasonable accuracy. However, they become computationally expensive with an increase in the number of notional particles (N_p) or the stochastic fields (N_{sf}).
5. A more recent numerical model, namely the multiple mapping conditioning (MMC) approach, has yielded promising numerical results for acetone flames of Sydney piloted spray burner⁸⁵. This generalized version of the MMC method based on sparse-Lagrangian MC technique used a significantly small number of particles as opposed to conventional composition FDF methods^{86,87}.
6. It is apparent that in most of the experimental setup of spray combustion, a significant amount of premixing takes place at the inlet or within a small region within the flow field. Therefore, the numerical models should be developed in a manner that they can be applied to non-premixed, premixed and partially premixed spray flames.
7. Further, numerical models are needed to predict the complex physical phenomena associated with dense sprays. For dense sprays, formulation of these turbulent combustion models needs to be developed and validated against experimental measurements. Thoroughly validated, accurate and efficient techniques for the numerical solution of combustion of sprays will help bridge information gaps in studies where the application of experimental methods is difficult.

List of symbols

B : Spalding transfer number; C_p : Specific heat at constant pressure; D : Diameter; E_a : Activation energy; g : Acceleration due to gravity; L_v : Latent heat of vaporization; Nu : Nusselt number; \mathcal{R}_u : Universal gas constant; P : Probability density function; q : Subgrid flux; Q : Conditional expectation; S_{ij} : Strain rate tensor; T : Temperature; v : Liquid phase velocity; W : Molecular weight; Y : Mass fraction; C : Reaction progress variable; C_{sgs} : Smagorinsky constant; \mathcal{D} : Diffusivity; G : LES filter function; h : Enthalpy; m : Mass; Re : Reynolds number; p : Gas phase pressure; Pr : Prandtl number; \dot{S} : Inter-phase transfer term due to droplet evaporation; Sc : Schmidt number; Sh : Sherwood number; u : Gas phase velocity; w : Weight of a notional particle; x : Spatial location; Z : Mixture fraction.

Greeks

α : Total reactive scalars (including enthalpy); Δ : LES filter width; δ : Dirac delta function; μ : Viscosity; τ : Timescale; $\dot{\omega}$: Reaction rate; β : Reactive scalars (without enthalpy); Δ_v : Filter volume; λ : Thermal conductivity; ρ : Density; τ_{ij} : Stress tensor.

Subscripts and superscripts

d: Droplet; g: Gas phase; p: Notional particle; sgs: Subgrid scale; F: Fuel; l: Liquid phase; sf: Stochastic fields.

Abbreviations

CMC: Conditional moment closure; ESF: Eulerian stochastic field; FPV: Flamelet progress variable; FSSF: Fully stochastic separated flow; MMC: Multiple mapping conditioning; PDF: Probability density function; SDE: Stochastic differential equation; DNS: Direct numerical simulation; FDF: Filtered density function; FGM: Flamelet-generated manifolds; LES: Large eddy simulation; MC: Monte Carlo; SGS: Subgrid scale; SPM: Stochastic particle method.

Publisher's Note

Springer Nature remains neutral with regard to jurisdictional claims in published maps and institutional affiliations.

Received: 6 February 2019 Accepted: 6 March 2019
Published online: 19 March 2019

References

- Jenny P, Roekaerts D, Beishuizen N (2012) Modeling of turbulent dilute spray combustion. *Prog Energy Combust Sci* 38:846–887
- Dukowicz JK (1980) A particle-fluid numerical model for liquid sprays. *J Comput Phys* 35:229–253
- Pitsch H (2005) Large-eddy simulation of turbulent combustion. *Annu Rev Fluid Mech* 38:453–482
- Burke SP, Schumann TEW (1928) Diffusion flames. *Ind Eng Chem* 20:998–1004
- Peters N (1984) Laminar diffusion flamelet models in non-premixed turbulent combustion. *Prog Energy Combust Sci* 10:319–339
- Bilger RW (1993) Conditional moment closure for turbulent reacting flow. *Phys Fluids A Fluid Dyn* 5:436–444
- Klimenko AY, Bilger RW (1999) Conditional moment closure for turbulent combustion. *Prog Energy Combust Sci* 25:595–687
- Ma L, Naud B, Roekaerts D (2016) Transported PDF modeling of ethanol spray in hot-diluted coflow flame. *Flow Turbul Combust* 96:469–502
- Chrigui M, Masri AR, Sadiki A, Janicka J (2013) Large eddy simulation of a polydisperse ethanol spray flame. *Flow Turbul Combust* 90:813–832
- Pope SB (1985) PDF methods for turbulent reactive flows. *Prog Energy Combust Sci* 11:119–192
- Jaberi FA, Colucci PJ, James S, Givi P, Pope SB (1999) Filtered mass density function for large-eddy simulation of turbulent reacting flow. *J Fluid Mech* 401:37
- Libby PA, Williams FA (1994) *Turbulent reacting flows*. Academic Press, London
- De S, Lakshmisha KN, Bilger RW (2011) Modeling of nonreacting and reacting turbulent spray jets using a fully stochastic separated flow approach. *Combust Flame* 158:1992–2008
- De S, Kim SH (2013) Large eddy simulation of dilute reacting sprays: droplet evaporation and scalar mixing. *Combust Flame* 160:2048–2066
- Ukai S, Kronenburg A, Stein OT (2014) Simulation of dilute acetone spray flames with LES-CMC using two conditional moments. *Flow Turbul Combust* 93:405–423
- Heye C, Raman V, Masri AR (2013) LES/probability density function approach for the simulation of an ethanol spray flame. *Proc Combust Inst* 34:1633–1641
- Ma L (2016) Computational modeling of turbulent spray combustion. Doctoral thesis, Delft University of Technology. <https://doi.org/10.4233/uuid:c1c27066-a205-45f4-a7b4-e36016bc313a>
- Masri AR, Gounder J, Kourmatzis A (2019) Experimental database, clean combustion research group, school of aerospace, mechanical and mechatronic engineering at the University of Sydney, Australia. <http://web.aeromech.usyd.edu.au/thermofluids/database.php>
- Gounder JD (2009) An Experimental Investigation of non-reacting and reacting spray jets. University of Sydney, Sydney
- O'Loughlin W, Masri AR (2011) A new burner for studying auto-ignition in turbulent dilute sprays. *Combust Flame* 158:1577–1590
- Smagorinsky J (1963) General circulation experiments with the primitive equations. *Mon Weather Rev* 91:99–164
- Germano M, Piomelli U, Moin P, Cabot WH (1991) A dynamic subgrid-scale eddy viscosity model. *Phys Fluids A Fluid Dyn* 3:1760–1765
- Lilly DK (1992) A Proposed modification of the germano subgrid-scale closure method. *Phys Fluids A Fluid Dyn* 4:633–635
- Nicoud F, Ducros F (1999) Subgrid-scale stress modelling based on the square of the velocity gradient tensor. *Flow Turbul Combust* 62:183–200
- Meneveau C, Lund TS, Cabot WH (1996) A Lagrangian dynamic subgrid-scale model of turbulence. *J Fluid Mech* 319:353
- Abramzon B, Sirignano WA (1989) Droplet vaporization model for spray combustion calculations. *Int J Heat Mass Transf* 32:1605–1618

27. Chrigui M, Gounder J, Sadiki A, Masri AR, Janicka J (2012) Partially premixed reacting acetone spray using LES and FGM tabulated chemistry. *Combust Flame* 159:2718–2741
28. Abramzon B, Sazhin S (2005) Droplet vaporization model in the presence of thermal radiation. *Int J Heat Mass Transf* 48:1868–1873
29. Crowe CT, Schwarzkopf JD, Sommerfeld M, Tsuji Y (2011) *Multiphase flows with droplets and particles*, 2nd edn. Taylor & Francis, New York
30. Faeth GM (1983) Evaporation and combustion of sprays. *Prog Energy Combust Sci* 9:1–76
31. Turn SR (2012) *Introduction to combustion: concepts and applications*, 3rd edn. McGraw-Hill, New York
32. Ukai S, Kronenburg A, Stein OT (2013) LES-CMC of a dilute acetone spray flame. *Proc Combust Inst* 34:1643–1650
33. Faeth GM (1977) Current status of droplet and liquid combustion. In: *Progress energy combustion science*, vol 3. Pergamon Press, pp 192–224
34. Faeth GM (1996) Spray combustion phenomena. *Symp Combust* 26:1593–1612
35. Apte SV, Mahesh K, Moin P (2009) Large-eddy simulation of evaporating spray in a coaxial combustor. *Proc Combust Inst* 32:2247–2256
36. Bilger RW (2011) A mixture fraction framework for the theory and modeling of droplets and sprays. *Combust Flame* 158:191–202
37. Pierce CD, Moin P (2004) Progress-variable approach for large-eddy simulation of non-premixed turbulent combustion. *J Fluid Mech* 504:73–97
38. Ihme M, Pitsch H (2008) Prediction of extinction and reignition in nonpremixed turbulent flames using a flamelet/progress variable model: 2. Application in LES of Sandia flames D and E. *Combust Flame* 155:90–107
39. Pitsch H (2007) FlameMaster: a C++ computer program for 0D combustion and 1D laminar flame calculations. <https://web.stanford.edu/group/pitsch/FlameMaster.htm>
40. Ma L, Roekaerts D (2016) Modeling of spray jet flame under MILD condition with non-adiabatic FGM and a new conditional droplet injection model. *Combust Flame* 165:402–423
41. Ma L, Roekaerts D (2017) Numerical study of the multi-flame structure in spray combustion. *Proc Combust Inst* 36:2603–2613
42. Eckstein J, Chen J-Y, Chou C-P, Janicka J (2000) Modeling of turbulent mixing in opposed jet configuration: one-dimensional Monte Carlo probability density function simulation. *Proc Combust Inst* 28:141–148
43. Cao RR, Pope SB, Masri AR (2005) Turbulent lifted flames in a vitiated coflow investigated using joint PDF calculations. *Combust Flame* 142:438–453
44. Mortensen M, Bilger RW (2009) Derivation of the conditional moment closure equations for spray combustion. *Combust Flame* 156:62–72
45. Bray KNC, Peters N (1994) Chapter-2 in *turbulent reacting flows*. Academic Press, London
46. Carbonell D, Perez-Segarra CD, Coelho PJ, Oliva A (2009) Flamelet mathematical models for non-premixed laminar combustion. *Combust Flame* 156:334–347
47. Ukai S (2014) Conditional moment closure modelling of turbulent spray flames. *ITV Stuttgart*
48. Navarro-Martinez S, Kronenburg A (2009) LES-CMC simulations of a lifted methane flame. *Proc Combust Inst*. <https://doi.org/10.1016/j.proci.2008.06.178>
49. Navarro-Martinez S, Kronenburg A, Di Mare F (2005) Conditional moment closure for large eddy simulations. *Flow Turbul Combust* 75:245–274
50. Sreedhara S, Lakshmisha KN (2002) Assessment of conditional moment closure models of turbulent autoignition using DNS data. *Proc Combust Inst* 29:2069–2077
51. Kronenburg A (2004) Double conditioning of reactive scalar transport equations in turbulent nonpremixed flames. *Phys Fluids* 16:2640–2648
52. Colucci PJ, Jaber FA, Givi P, Pope SB (1998) Filtered density function for large eddy simulation of turbulent reacting flows. *Phys Fluids* 10:499–515
53. Khan MN, Cleary MJ (2017) Sparse-Lagrangian MMC-LES modelling of reacting acetone spray. In: *11th Asia-Pacific Conf. Combust.*
54. Haworth DC (2010) Progress in probability density function methods for turbulent reacting flows. *Prog Energy Combust Sci* 36:168–259
55. Fox RO (2003) *Computational models for turbulent reacting flows*. Cambridge University Press. <https://doi.org/10.1017/CBO9780511610103>
56. Prasad VN, Masri AR (2012) LES calculations of autoignition in a turbulent dilute methanol spray flame 18–21
57. Heye C, Raman V, Masri AR (2015) Influence of spray combustion interactions on auto-ignition of methanol spray flames. *Proc Combust Inst* 35:1639–1648. <https://doi.org/10.1016/j.proci.2014.06.087>
58. Jones WP, Lyra S, Marquis AJ (2010) Large eddy simulation of evaporating kerosene and acetone sprays. *Int J Heat Mass Transf* 53:2491–2505
59. Pope SB (2000) *Turbulent flows*, 1st edn. Cambridge University Press, New York. <https://doi.org/10.1088/0957-0233/12/11/705>
60. Gao F, O'Brien EE (1993) A large-eddy simulation scheme for turbulent reacting flows. *Phys Fluids A Fluid Dyn* 5:1282–1284
61. Janicka J, Kolbe W, Kollmann W (1979) Closure of the transport equation for the probability density function of turbulent scalar fields. *J Non-Equilib Thermodyn* 4:47–66
62. Dopazo C, O'Brien EE (1974) An approach to the autoignition of a turbulent mixture. *Acta Astronaut* 1:1239–1266
63. Pope SB (1981) A monte carlo method for the pdf equations of turbulent reactive flow. *Combust Sci Technol* 25:159–174

64. Pope SB (1990) Computations of turbulent combustion: progress and challenges. *Proc Combust Inst* 23:591–612
65. James S, Anand M, Pope SB (2002) The Lagrangian PDF transport method for simulations of gas turbine combustor flows. In: 38th AIAA/ASME/SAE/ASEE Jt Propuls Conf & Exhib 2002
66. Jones WP, Lyra S, Navarro-Martinez S (2012) Numerical investigation of swirling kerosene spray flames using large eddy simulation. *Combust Flame* 159:1539–1561
67. Valiño L (1998) A field Monte Carlo formulation for calculating the probability density function of a single scalar in a turbulent flow. *Flow Turbul Combust* 60:157–172
68. Möbus H, Gerlinger P, Brüggemann D (2001) Comparison of Eulerian and Lagrangian Monte Carlo PDF methods for turbulent diffusion flames. *Combust Flame* 124:519–534
69. Jones WP, Marquis AJ, Vogiatzaki K (2014) Large-eddy simulation of spray combustion in a gas turbine combustor. *Combust Flame* 161:222–239
70. Sabel'nikov V, Soularo O (2005) Rapidly decorrelating velocity-field model as a tool for solving one-point Fokker-Planck equations for probability density functions of turbulent reactive scalars. *Phys Rev E Stat Nonlinear Soft Matter Phys* 72:016301
71. Gounder JD (2010) Turbulent spray flames of acetone and ethanol approaching extinction AU—masri. *A R Combust Sci Technol* 182:702–715
72. Gounder JD, Kourmatzis A, Masri AR (2012) Turbulent piloted dilute spray flames: flow fields and droplet dynamics. *Combust Flame* 159:3372–3397
73. O'Loughlin W, Masri AR (2012) The structure of the auto-ignition region of turbulent dilute methanol sprays issuing in a vitiated co-flow. *Flow Turbul Combust* 89:13–35
74. Cavaliere DE, Kariuki J, Mastorakos E (2013) A comparison of the blow-off behaviour of swirl-stabilized premixed, non-premixed and spray flames. *Flow Turbul Combust* 91:347–372
75. Karpets AN, Gomez A (2000) An experimental study of well-defined turbulent nonpremixed spray flames. *Combust Flame* 121:1–23
76. Renou B, Cabot G, Marrero J, Verdier A (2017) Coria jet spray flame database 1–3
77. Shum-Kivan F, Marrero Santiago J, Verdier A, Riber E, Renou B, Cabot G et al (2017) Experimental and numerical analysis of a turbulent spray flame structure. *Proc Combust Inst* 36:2567–2575
78. Verdier A, Santiago JM, Vandel A, Godard G, Cabot G, Boukhalfa MA et al (2016) Experimental study of local extinction mechanisms on a spray jet flame. In: 18th Int Symp Appl Laser Imaging Tech to Fluid Mech 2016
79. Correia Rodrigues H, Tummers MJ, van Veen EH, Roekaerts DJEM (2015) Spray flame structure in conventional and hot-diluted combustion regime. *Combust Flame* 162:759–773
80. Rodrigues HRC, Tummers MJ, Roekaerts D (2013) Turbulent spray combustion in hot-diluted co-flow. In: Proc 9th Asia-Pacific conf combust 2013
81. Ukai S, Kronenburg A, Stein OT (2015) Large eddy simulation of dilute acetone spray flames using CMC coupled with tabulated chemistry. *Proc Combust Inst* 35:1667–1674
82. Klein M, Sadiki A, Janicka J (2003) A digital filter based generation of inflow data for spatially developing direct numerical or large eddy simulations. *J Comput Phys* 186:652–665
83. Prasad VN, Masri AR, Navarro-Martinez S, Luo KH (2013) Investigation of auto-ignition in turbulent methanol spray flames using Large Eddy Simulation. *Combust Flame* 160:2941–2954
84. Pope SB (1997) Computationally efficient implementation of combustion chemistry using in situ adaptive tabulation (ISAT). *Combust Theory Model* 1:41–63
85. Khan N, Cleary MJ, Stein OT, Kronenburg A (2018) A two-phase MMC-LES model for turbulent spray flames. *Combust Flame* 193:424–439
86. Klimenko AY, Pope SB (2003) The modeling of turbulent reactive flows based on multiple mapping conditioning. *Phys Fluids* 15:1907–1925
87. Cleary MJ, Klimenko AY (2009) A generalised multiple mapping conditioning approach for turbulent combustion. *Flow Turbul Combust* 82:477–491



Eshan Sharma is a Ph.D. research scholar at the Indian Institute of Technology, Kanpur. His research interests include large eddy simulations, primary atomisation and reactive spray modeling.



Santanu De is an Assistant Professor in the Mechanical Engineering, IIT Kanpur, since December 2014. He received a Bachelor of Engineering from the North Bengal University in 2002 and an M.Tech. from the IIT Kanpur in 2004, both in Mechanical Engineering. He received his Ph.D. in Aerospace

Engineering from the Indian Institute of Science, Bangalore, in 2012. Prior to his joining at IIT Kanpur, he served as a postdoctoral research associate at the Michigan Technological University and at the Institute of Combustion Technology (ITV), University of Stuttgart. He also worked as a Scientist at the Liquid Propulsion Systems Centre, Indian Space Research Organization, between 2004 and 2005. His primary areas of research are numerical modelling of turbulent combustion, spray atomization and combustion, coal gasification and gas turbine combustion. He is an editorial board member of the 'Journal of Energy, Environment and Sustainability.'